

Article

Analytical Fragility Surfaces and Global Sensitivity Analysis of Buried Operating Steel Pipeline Under Seismic Loading

Gersena Banushi 

Department of Civil and Environmental Engineering, University of California, Berkeley, Berkeley, CA 94720, USA; g.banushi@berkeley.edu

Abstract: The structural integrity of buried pipelines is threatened by the effects of Permanent Ground Deformation (PGD), resulting from seismic-induced landslides and lateral spreading due to liquefaction, requiring accurate analysis of the system performance. Analytical fragility functions allow us to estimate the likelihood of seismic damage along the pipeline, supporting design engineers and network operators in prioritizing resource allocation for mitigative or remedial measures in spatially distributed lifeline systems. To efficiently and accurately evaluate the seismic fragility of a buried operating steel pipeline under longitudinal PGD, this study develops a new analytical model, accounting for the asymmetric pipeline behavior in tension and compression under varying operational loads. This validated model is further implemented within a fragility function calculation framework based on the Monte Carlo Simulation (MCS), allowing us to efficiently assess the probability of the pipeline exceeding the performance limit states, conditioned to the PGD demand. The evaluated fragility surfaces showed that the probability of the pipeline exceeding the performance criteria increases for larger soil displacements and lengths, as well as cover depths, because of the greater mobilized soil reaction counteracting the pipeline deformation. The performed Global Sensitivity Analysis (GSA) highlighted the influence of the PGD and soil–pipeline interaction parameters, as well as the effect of the service loads on structural performance, requiring proper consideration in pipeline system modeling and design. Overall, the proposed analytical fragility function calculation framework provides a useful methodology for effectively assessing the performance of operating pipelines under longitudinal PGD, quantifying the effect of the uncertain parameters impacting system response.

Keywords: steel pipeline; longitudinal ground movement; fragility surfaces; Monte Carlo Simulation (MCS); Global Sensitivity Analysis (GSA); uncertainty quantification; operational loads



Citation: Banushi, G. Analytical Fragility Surfaces and Global Sensitivity Analysis of Buried Operating Steel Pipeline Under Seismic Loading. *Appl. Sci.* **2024**, *14*, 10735. <https://doi.org/10.3390/app142210735>

Academic Editor: Giuseppe Lacidogna

Received: 21 September 2024
Revised: 15 November 2024
Accepted: 15 November 2024
Published: 20 November 2024



Copyright: © 2024 by the author. Licensee MDPI, Basel, Switzerland. This article is an open access article distributed under the terms and conditions of the Creative Commons Attribution (CC BY) license (<https://creativecommons.org/licenses/by/4.0/>).

1. Introduction

Buried continuous pipelines are vulnerable to the effects of Permanent Ground Deformation (PGD) resulting from seismic-induced landslides, faulting, and lateral spreading due to liquefaction. The pipeline response depends on its orientation with respect to the direction of the ground movement, which is generally a combination of transverse and longitudinal ground movement, occurring perpendicular and parallel to the pipeline axis, respectively. Transverse PGD induces predominant shear and bending stresses at the margins of the PGD zone, similar to the fault-crossing problem investigated by many researchers during the last 50 years [1–5]. Conversely, the longitudinal PGD results in axial compression and tension in the pipeline that may ultimately lead to local buckling and tensile rupture, respectively. According to previous investigations [6–9], buried continuous pipelines are significantly more vulnerable to PGD in the longitudinal direction, requiring a detailed analysis of the system performance under this hazard.

The response of buried continuous pipelines subjected to longitudinal PGD depends on the pipe deformation capacity under operating conditions, as well as the soil–structure

interaction, amount of ground movement δ and its spatial extent L_b , and pattern of ground deformation (Figure 1).

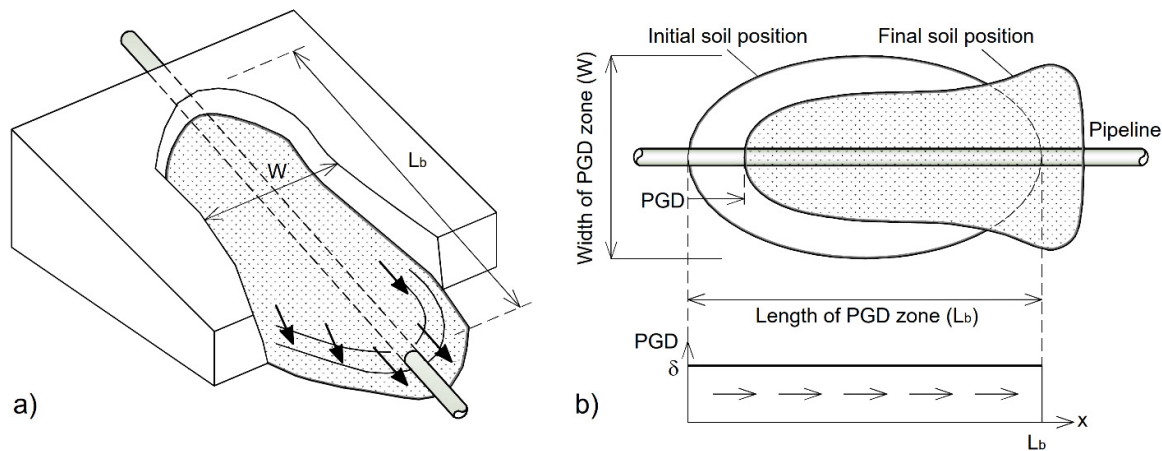


Figure 1. Pipeline subjected to longitudinal PGD: (a) 3D view; (b) 2D schematic representation.

The rigid block pattern, defined by a downslope movement δ within the soil block length L_b , induces localized relative soil–pipeline displacement at the margins, resulting in the largest pipe strains when compared to other distributive geometries considered by O’Rourke and Nordberg [7]. Consequently, this pattern has been extensively employed within simple analytical or more complex numerical methods to assess pipeline performance under longitudinal PGD [7,10–19].

These analytical structural models are more computationally efficient, compared to a complex numerical analysis approach, which requires further expertise of the engineer to analyze the models for use in routine engineering applications [20].

The existing analytical models for assessing the deformation of buried continuous pipelines subjected to longitudinal PGD consider the pipe material either as linear elastic [7,10] or inelastic, following a Ramberg–Osgood stress–strain relationship that is equal in tension and compression [8,11,19]. Herein, two conditions were established for which the pipeline deformation demand was assessed, depending on whether the soil block length L_b is short (case I) or long enough (case II) to fully mobilize the soil reaction along the pipeline under the imposed ground displacement (Figure 2). The pipeline design force was computed as the minimum between the ultimate soil reaction transferable to the pipe over a length of $L_b/2$ (case I) and the force computed assuming that the pipeline is fully compliant with the soil (case II), as recommended by the 2005 ALA guideline [12]. This conventional model predicts that half the total applied soil load is resisted in tension and half in compression, because of the assumed symmetric configuration of the soil–pipeline system, including the material constitutive relationships in tension and compression. Consequently, for a given PGD demand (d, L_b), the estimated peak pipeline strain magnitude in tension is equal to that in compression, as shown in Figure 2. This is not representative of pipelines made of materials with different stress–strain relationships for tension and compression under uniaxial or biaxial stress state conditions, resulting in asymmetric pipeline loading and strain demand in the tensile and compressive ground deformation zone.

Therefore, to accurately assess pipeline performance under longitudinal PGD, it is necessary to adopt analytical methods considering the asymmetric nonlinear material behavior of the operating pipeline for tension and compression as well as the elastoplastic axial soil–pipeline interaction [5,21].

Analytical models can be efficiently implemented within a seismic fragility analysis framework to evaluate the structural performance considering the uncertainties of the system parameters. Pipeline fragility assessments require proper consideration of the variability of the physical characteristics of the soil–pipe system, including the material

strength properties, the soil cover depth, and the pipe operational loads such as temperature differences and internal pressure [22–25].

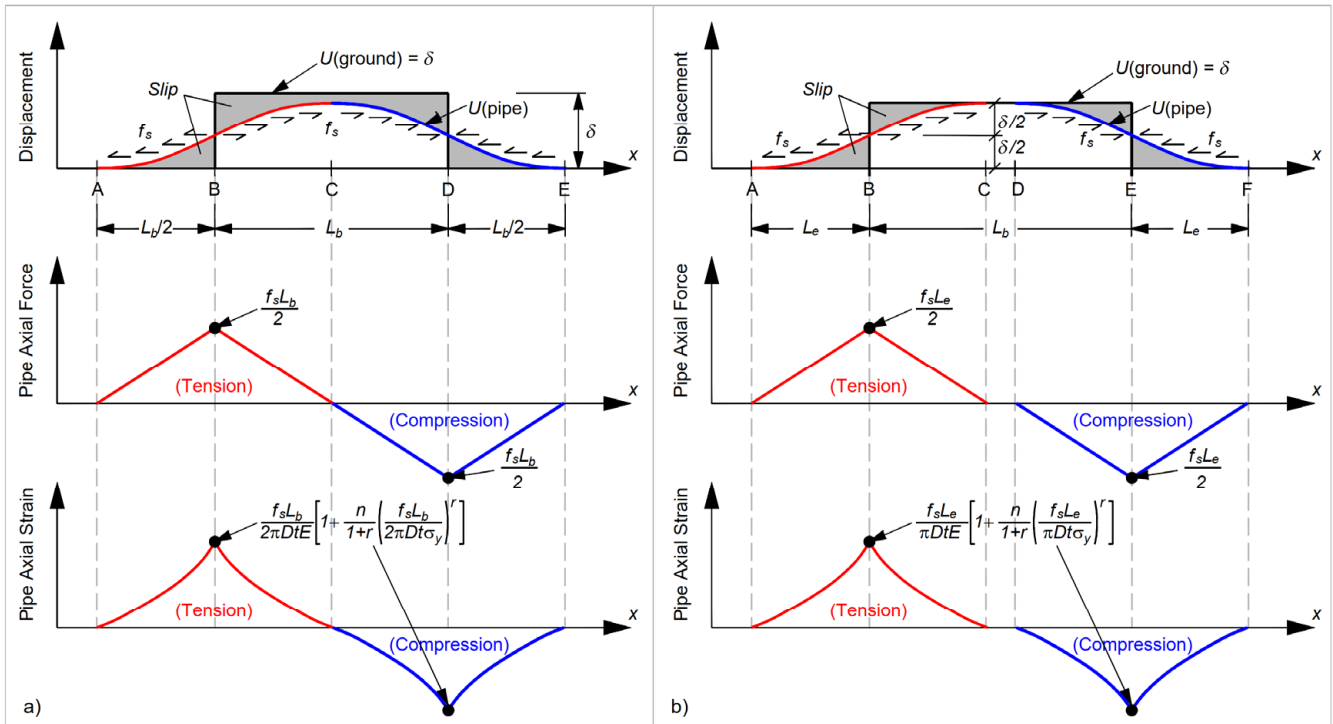


Figure 2. Pipeline response to longitudinal PGD according to analytical model in [11], assuming symmetric material behavior for tension and compression: (a) case I; (b) case II.

These uncertainties are considered within a probabilistic framework like the Monte Carlo Simulation (MCS), employing a large number of soil–pipeline system samples, generated by random sampling of the input system parameters, based on their probability distribution.

The seismic demands are compared to the structural capacity values associated with a certain performance limit state, allowing to estimate the associated probability of exceedance as a function of the level of seismic intensity measure, IM [26,27]. The latter is defined by a group of representative seismic ground motion parameters, e.g., the peak ground displacement δ , and the length of the PGD zone L_b . Conversely, the structural limit states are defined on the basis of an adequate Engineering Demand Parameter (EDP), e.g., the peak longitudinal strain, describing the system performance [28,29].

The analytical fragility relationships represent a useful design tool, allowing us to identify precise locations of pipeline damage, which is fundamental in evaluating pipeline seismic performance and prioritizing resource allocation for mitigative or remedial measures in spatially distributed lifeline systems.

To efficiently evaluate the seismic fragility of buried operating steel pipelines under longitudinal PGD, this study developed a new analytical model considering the asymmetric nonlinear response of the operating pipeline for tension and compression. The proposed model was validated through detailed finite element analysis, demonstrating its capacity to accurately evaluate pipeline system response under varying operational and seismic loads. The analytical formulation was further implemented within a fragility function calculation framework based on a Monte Carlo Simulation (MCS), assessing the probability of the pipeline exceeding the performance limit states, conditioned to the ground displacement hazard. Furthermore, to quantify the influence of the uncertain input parameters on the predicted pipeline performance, this study conducted Global Sensitivity Analysis (GSA), based on the Sobol’s variance decomposition method, using MCS to calculate the Sobol’s sensitivity indices.

First, this paper presents the methodology adopted to evaluate the seismic fragility of buried pipelines subjected to longitudinal PGD, using an accurate analytical model considering the asymmetric pipeline material behavior for tension and compression under varying service loads.

Then, the obtained fragility analysis results are carefully discussed and compared to data reported in other research publications, highlighting the main factors influencing the seismic performance of buried operating pipelines, considering the system uncertainties. Finally, the conclusion section highlights the contributions of the present paper to the state-of-the-art practice and research of pipeline seismic design, suggesting further important perspectives related to the addressed issues.

2. Methodology

This section presents the adopted methodology to assess the seismic fragility of buried operating pipelines subjected to longitudinal PGD. First, the developed analytical model is described, allowing us to evaluate the performance of buried operating pipelines under longitudinal PGD, as a function of the system nonlinearities and operational loads. Second, it defines the pipeline performance limit states evaluated through structural analysis. Then, the analytical model results are compared to the finite element analysis results, demonstrating the validity of the proposed analytical procedure. Finally, this section presents a probabilistic framework, based on Monte Carlo Simulation (MCS), to evaluate the fragility functions and quantify the effect of system uncertainties.

2.1. Analytical Model for Assessment of the Continuous Pipeline Response Under Longitudinal PGD

This section describes the developed analytical model for assessing the performance of buried continuous pipelines under longitudinal PGD, considering the nonlinear material constitutive relationships, force equilibrium, and displacement compatibility along the pipe–soil system. This algorithm allows implementation of the asymmetric nonlinear stress–strain relationship for the pipe material for tension and compression, as well as the elastoplastic axial soil–pipeline interaction, accurately assessing the response of the system subjected to this geohazard.

The ground deformation is idealized as a rigid-block movement, defined by a downslope movement δ over a block length L_b , resulting in a tension crack of width δ at the upslope end and a compression ridge over a distance δ on the downslope end (Figure 3a). The soil displacement assumes a constant value δ within the PGD zone, while being zero on either side of it.

The moving soil block tends to pull the pipe along with it, resulting in localized relative soil–pipeline displacement at the margins of the PGD zone, and associated resistance forces on either side of the sliding block head and toe. This results in a maximum pipeline axial force at the head and maximum axial compression force at the toe, decreasing linearly thereupon due to the sliding soil friction (f_s). Beyond this zone, the relative soil–pipeline displacement is negligible, and the pipeline displacement matches that of the ground (case II). As the soil displacement increases reaching a critical value $\delta = \delta_{cr}$, the relative soil–pipeline displacement and associated friction reaction are mobilized over the entire soil block length, and the pipeline deformation remains constant thereafter (case I).

Evidently, the region of the soil–pipeline system beyond the soil block behaves like a pull-out test under tension (region I) and compression (region IV), with the end displacement (ΔL) applied at the pipe points underlying the tension crack and compression bulge, respectively (Figure 3a). The total pipeline elongation at each side of the soil block head i.e., in region I (U_{p1}) and region II (U_{p2}), is equal to the magnitude of the overall pipeline contraction at each side of the toe of the sliding block, i.e., in region III (U_{p3}) and region IV (U_{p4}).

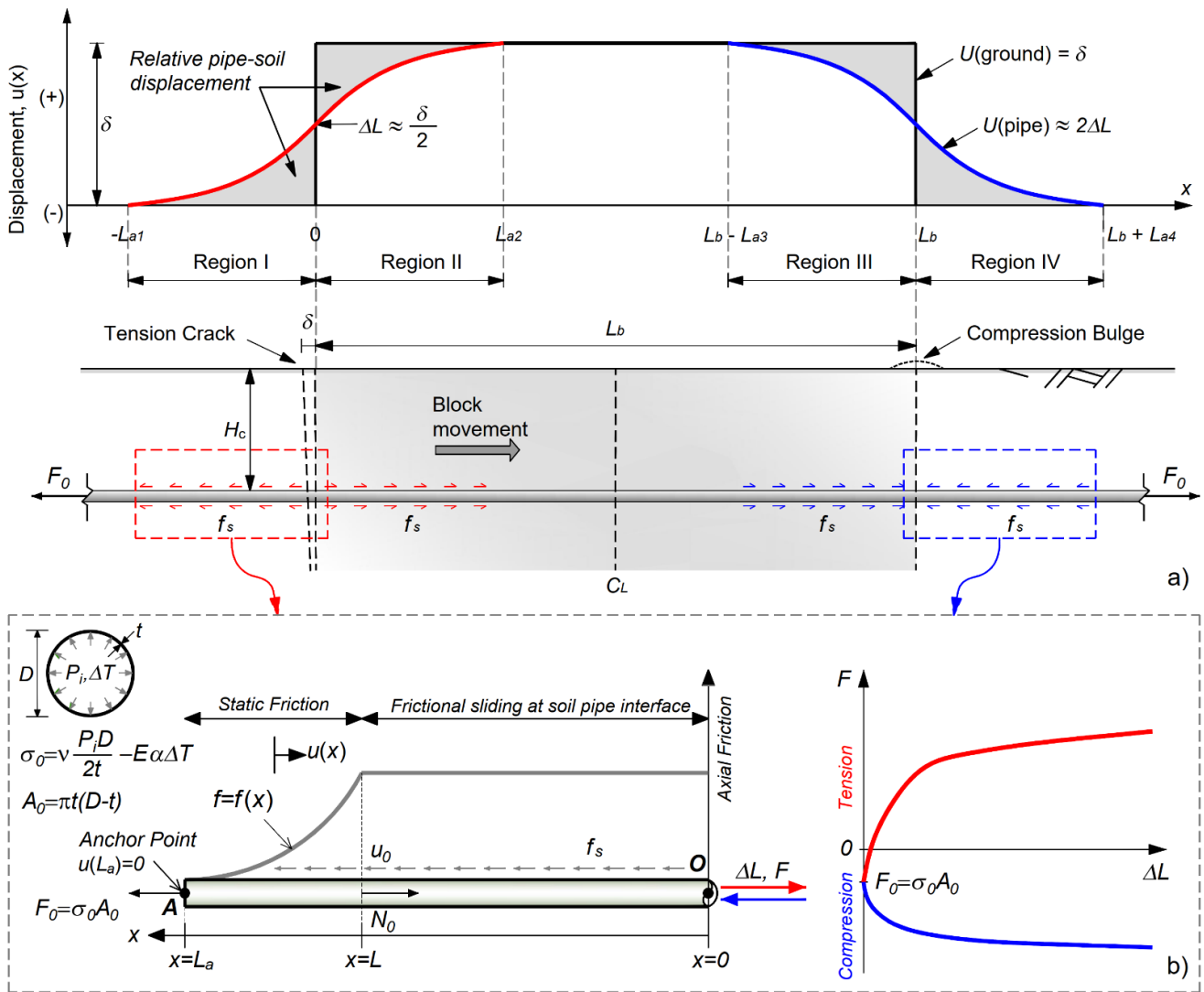


Figure 3. Schematic representation of operating pipeline response subjected to longitudinal PGD: (a) pipeline displacement subjected to longitudinal soil block movement (case II); (b) soil–pipeline system behaving like a pull-out test under tension (region I) and compression (region IV).

The strain demand was calculated using the analytical model developed by [30], evaluating the structural response of a continuous buried pipeline, subjected to a pullout force on one end ($x = 0$). The resulting pipeline displacement was obtained by integrating the axial strains associated with the axial force distribution along the pipeline, considering the beam on elastic foundation theory for the static friction length, and the force equilibrium for the frictional sliding length (Figure 3b). This model employs the theory of plasticity for modeling the pipe material, based on the associated flow rule with the von Mises yield criterion and isotropic strain hardening. Compared to the conventional model [8], the proposed analytical solution accounts for the initial axial thermal strains and biaxial stress state in the pipe due to internal pressure, as shown in Figure 4.

Herein, the pipe material is assumed to have a piecewise stress–strain curve, defined by the engineering strain–stress values (ϵ_i, σ_i) , either in tension ($\epsilon > 0$) or in compression ($\epsilon < 0$), where $E_i = (\sigma_i - \sigma_{i-1}) / (\epsilon_i - \epsilon_{i-1})$ is the slope of the i -th segment constituting the pipe multi-linear stress–strain relationship (Figure 4). Assuming the plastic behavior of the pipe steel material within the Von Mises plasticity with isotropic hardening (Figure 4), the nominal stress–strain curve (ϵ_i, σ_i) is derived from the true strain–true stress response $(\epsilon_{t,i}, \sigma_{t,i})$, as a function of the tensile coupon test data in terms of true strain and true stress $(\epsilon^{\circ}_i, \sigma^{\circ}_i)$, as well as the operating loads, as indicated in Table 1. Herein, $\sigma_{\theta} = P_i D / 2t$

denotes the hoop stress in the pressurized pipeline, E the Young’s modulus of the pipe material, ν the Poisson’s ratio, $E_i^\circ = (\sigma_i^\circ - \sigma_{i-1}^\circ)/(\varepsilon_i^\circ - \varepsilon_{i-1}^\circ)$ the tangent modulus of the i -th segment constituting the pipe multi-linear true stress–true strain relationship, and $H_i^\circ = E \cdot E_i^\circ / (E - E_i^\circ)$ the plastic modulus of the true stress–true plastic strain curve (flow curve).

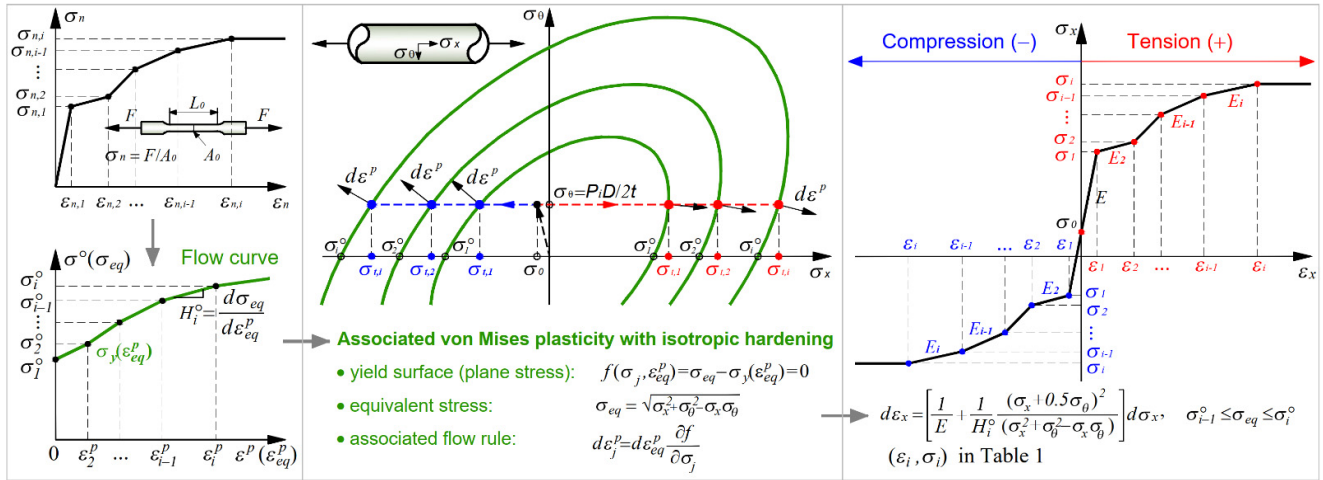


Figure 4. Schematic representation of the axial constitutive behavior of the steel pipe material, defined within the associated von Mises plasticity with isotropic hardening [30].

Table 1. Closed-form analytical solution for the axial true stress–true strain response of the steel pipeline subjected to internal pressure P_i and temperature variations ΔT [30].

i	$\sigma_{t,i}$	$\varepsilon_{t,i}$
0	$\sigma_0 = \nu\sigma_\theta - E\alpha\Delta T$	$\varepsilon_0 = 0$
1	$\sigma_{t,1} = \sigma_\theta/2 \pm \sqrt{(\sigma_1^\circ)^2 - 3\sigma_\theta^2/4}$	$\varepsilon_{t,1} = \varepsilon_0 + \frac{\sigma_{t,1} - \sigma_0}{E}$
>1	$\sigma_{t,i} = \sigma_\theta/2 \pm \sqrt{(\sigma_i^\circ)^2 - 3\sigma_\theta^2/4}$	$\varepsilon_{t,i} = \varepsilon_{t,i-1} + \frac{(\sigma_{t,i} - \sigma_{t,i-1})}{E_i^\circ} - \frac{\sqrt{3}\sigma_\theta}{2H_i^\circ} \arctan\left(\frac{2\sqrt{3}\sigma_\theta(\sigma_{t,i} - \sigma_{t,i-1})}{3\sigma_\theta^2 + (2\sigma_{t,i} - \sigma_\theta)(2\sigma_{t,i-1} - \sigma_\theta)}\right)$

The pipe–soil interaction is modeled using an elastic–perfectly plastic force–displacement relationship, defined by the maximum soil friction force per unit length of the pipeline f_s , and the relative soil–pipeline displacement at onset of friction sliding u_0 , where $k = f_s/u_0$ is the rigidity of friction interaction.

The analytical formulation for evaluating the buried pipeline displacement ΔL subjected to a pull-out force at the head ($F = F_{t,max}$) and toe ($F = F_{c,max}$) of the sliding soil block is indicated in Table 2. Herein, the unanchored length (L_a) of the pipeline is assumed to be sufficiently long so that the pipeline response is unaffected by far-end boundary conditions.

Table 2. The analytical formulation for evaluating the pipeline response ($\Delta L, F$) at the head and toe of the soil block, behaving like a pull-out test for tension (+) and compression (−), respectively [30].

i	F -Interval	Pipe Displacement ΔL	Pipe Axial Force F
1	$ F - A\sigma_0 \leq \sqrt{AEf_s u_0}$ $A\sigma_1^- \leq F \leq A\sigma_1^+$	$\pm \sqrt{AE_1/k} \cdot \varepsilon$ $\pm \frac{u_0}{2} \pm \frac{AE_1}{2f_s} \varepsilon^2$	$A\sigma_0 + AE_1(\varepsilon - \varepsilon_0)$
>1	$F < A\sigma_1^- \vee F > A\sigma_1^+$	$\Delta L_{i-1} \pm \frac{AE_i}{2f_s} (\varepsilon^2 - \varepsilon_{i-1}^2)$	$A\sigma_{i-1} + AE_i(\varepsilon - \varepsilon_{i-1})$

The magnitude of the total pipeline displacement under tension ($U_{p,max} = U_{p1} + U_{p2} \cong 2\Delta L$) and compression ($U_{p,max} = U_{p3} + U_{p4} \cong 2\Delta L$) are equal to the ground displacement δ until

the soil friction mobilizes over the entire soil block (case II), remaining constant thereafter, $U_{p,max} = \delta_{cr} - u_0$ (case I). This allows us to directly assess the amount of ground displacement δ inducing a maximum pipeline strain ε either in tension or compression, at the soil block head and toe, respectively, using the following equation:

$$\delta(\varepsilon) = 2\Delta L(\varepsilon), \quad \text{for } \delta < \delta_{cr} \quad (1)$$

The evaluation of the critical soil displacement δ_{cr} as a function of the soil block length L_b is described in detail in Section 2.4. Most importantly, Equation (1) allows us to determine the amount of critical ground displacement ($\delta_{cr,i}$) corresponding to the achievement of the level of pipe axial strain associated with a certain performance limit state, either for tension or compression.

2.2. Deformation Capacity and Performance Limit States for the Steel Pipeline

In this study, the pipeline response was assessed in terms of the critical ground displacement corresponding to the achievement of maximum allowable longitudinal compression and tension strains, associated with normal operability and pressure integrity performance goal.

2.2.1. Normal Operability Limit (NOL) State

It is expected that the pipeline will maintain its functionality after a seismic event, and the induced longitudinal strains are limited to avoid excessive distortion of the pipe cross-section impairing the passage of internal pigs for cleaning and inspections for material leakage. According to the 2001 ALA Guideline [31], the longitudinal compression strain limit, associated with the onset of local buckling, is given by the following:

$$\varepsilon_{c1} = 0.5 \frac{t}{D'} + 3000 \left(\frac{pD}{2Et} \right)^2 - 0.0025 \quad (2)$$

with,

$$D' = \frac{0.5D}{1 - \frac{3}{D}(D - D_{min})}, \quad (3)$$

where p is the difference between the pipe internal and external pressure, E is the elastic modulus of the pipe material, t is the pipeline thickness, D is the pipeline diameter, and D_{min} is minimum pipe diameter because of ovalization.

To maintain normal operability, the 2001 ALA Guideline recommends limiting the magnitude of longitudinal tensile strain to $\varepsilon_{t1} = 2\%$.

2.2.2. The Pressure Integrity Limit (PIL) State

It accepts significant pipe ovalization and wrinkle formation without loss of containment, which may subsequently result in pipe wall folding and associated excessive tensile strains, leading to crack initiation and ultimate rupture. To guarantee the pressure integrity performance requirement, the longitudinal compressive strain limit was evaluated as $\varepsilon_{c2} = 1.76 t/D$. The allowable longitudinal tensile strain limit was assumed to be $\varepsilon_{t2} = 4\%$ [31,32].

Evidently, the pipeline performance is controlled by its compressive behavior, being the magnitude of the strain limit for normal operability (NOL) for compression lower than that for tension ($\varepsilon_{c1} < \varepsilon_{t1}$), for typical ranges of the diameter-to-thickness ratio (D/t) in onshore applications.

2.3. Validation of the Analytical Model

The proposed analytical model was validated against numerical simulation evaluating the response of buried operating pipeline under longitudinal PGD, using the finite element software ABAQUS/Standard [33]. First, the system performance was analyzed numerically within the beam on Winkler foundation theory. Then, the numerical results were compared

to those obtained using the state-of-the-art analytical procedure [8,11,13] and the proposed analytical model, demonstrating the capacity of the latter to accurately evaluate the pipeline response.

The calculation example considers a X42 steel grade pipeline with diameter of 0.508 m and thickness of 7.1 mm, buried in dense sand with a cover depth $H_c = 1.5$ m, measured from the soil surface to the pipe crown. The analyzed soil–pipeline parameters are summarized in Table 3.

Table 3. Pipe–soil system parameters.

Parameter	Value	Units
Pipe diameter, D	0.508	m
Pipe wall thickness, t	7.1	mm
Pipe elastic modulus, E	210	GPa
Poisson's ratio, ν	0.3	
Pipe yield stress, σ_y	290	MPa
Pipe cover depth, H_c	1.5	m
Soil density, γ	18.0	kN/m ³
Soil friction angle, ϕ	40	°
Pipe–soil interface friction angle, δ_i	28	°
Soil pressure at rest, K_0	1	
Soil friction reaction per unit pipe length, f_s	26.8	kN/m
Relative soil–pipe displacement at friction sliding, u_0	3	mm

The pipeline performance was evaluated considering the presence and absence of service loads, including internal pressure P_i , and temperature variations ΔT , demonstrating the accuracy of the proposed analytical method to assess the system response under operating conditions.

It is assumed that the unpressurized pipeline ($P_i = 0$ MPa) has no temperature variation with respect to its installation temperature ($\Delta T = 0$ °C). Conversely, the pressurized pipeline is assumed to operate at an average temperature of $\Delta T = 50$ °C, compared to the pipe installation temperature, and internal pressure $P_i = 4.4$ MPa, which is 75% of the maximum allowed pressure, P_{max} , according to [34]:

$$P_{max} = 0.72 \cdot \left(2\sigma_y \frac{t}{D} \right) \quad (4)$$

2.3.1. Finite Element Analysis of the Soil–Pipeline System

Within the numerical approach, the pipeline was modeled using the PIPE22H beam element type implemented in Abaqus/Standard [33], which is particularly suitable to model long, slender pipelines with a thin-walled circular cross-section, allowing the possibility of specifying external or internal pressures. Instead, the longitudinal soil–pipeline interaction was modeled with uniaxial spring elements SPRING2 connected at each node of the pipeline on one end, while being assigned the far-field ground motion at the other end through the boundary conditions. The adopted mesh size for the beam pipe elements is 0.10 m, based on the mesh sensitivity study performed herein, assuring efficiency and accuracy of the numerical solution.

The X42 steel grade pipe material model is defined within the von Mises plasticity theory with isotropic hardening, with Young modulus $E = 210$ GPa, and yield stress $\sigma_y = 290$ MPa. The elasto-plastic force displacement relationship of the soil springs is defined by the sliding soil friction force per unit length of the pipeline, $f_s = 26.8$ kN/m, and the relative soil–pipe displacement at the onset of friction sliding, $u_0 = 3$ mm, calculated according to the ALA guidelines [31], assuming compacted dense sand with friction angle $\phi = 40^\circ$ (Table 3).

The length of the pipeline–soil system is equal to 1000 m, so the system response to the imposed ground displacement is representative of an infinitely long pipeline, unaf-

ected by the far-end boundary conditions. The assumed soil block length is $L_b = 300$ m (case II), located at the center of the soil–pipeline system so that its midpoint lies on the pipeline bisector.

The numerical analysis was conducted in two consecutive steps. First, the internal pressure and temperature variations were applied in the pipeline, while the pipeline ends and the free ends of the soil springs were restrained in the longitudinal direction. Second, the soil block movement $\delta = 4$ m was applied statically with a maximum step increment equal to $\Delta\delta = 1$ mm at the free nodes of the soil springs within the soil block length, while outside of the moving block the soil nodes remain fixed. At each step increment, the nonlinear equilibrium equations were solved iteratively by the Newton–Raphson method, allowing us to assess the system performance at any level of applied ground displacement, until material failure.

2.3.2. Comparison Between Numerical and Analytical Solutions

Figure 5 shows a comparison between the numerical and analytical model results assessing the performance of the pressurized and unpressurized pipelines in terms of the maximum axial strains for tension and compression, as a function of the ground displacement δ . Overall, the peak pipe strain magnitudes in the tensile and compressive PGD zone increase monotonically with the ground movement, progressively reaching the NOL and PIL performance limit states at critical values of ground displacement $\delta_{cr,i}$, based on the operating conditions (Table 4).

The results obtained using the conventional model reported in [8,11,13] agree well with the numerical analysis only for the case of the unpressurized pipeline under tension, while diverging significantly for the pressurized pipeline, with a percent difference exceeding 5% (Table 4). Conversely, the comparison between the proposed analytical model and the numerical simulation results shows excellent agreement for both cases of pipeline operating conditions. Specifically, the percent difference between the pipeline performance results for these two methods does not exceed 0.9% (Table 4), demonstrating the greater accuracy of this analytical procedure to assess system response, compared to the conventional method.

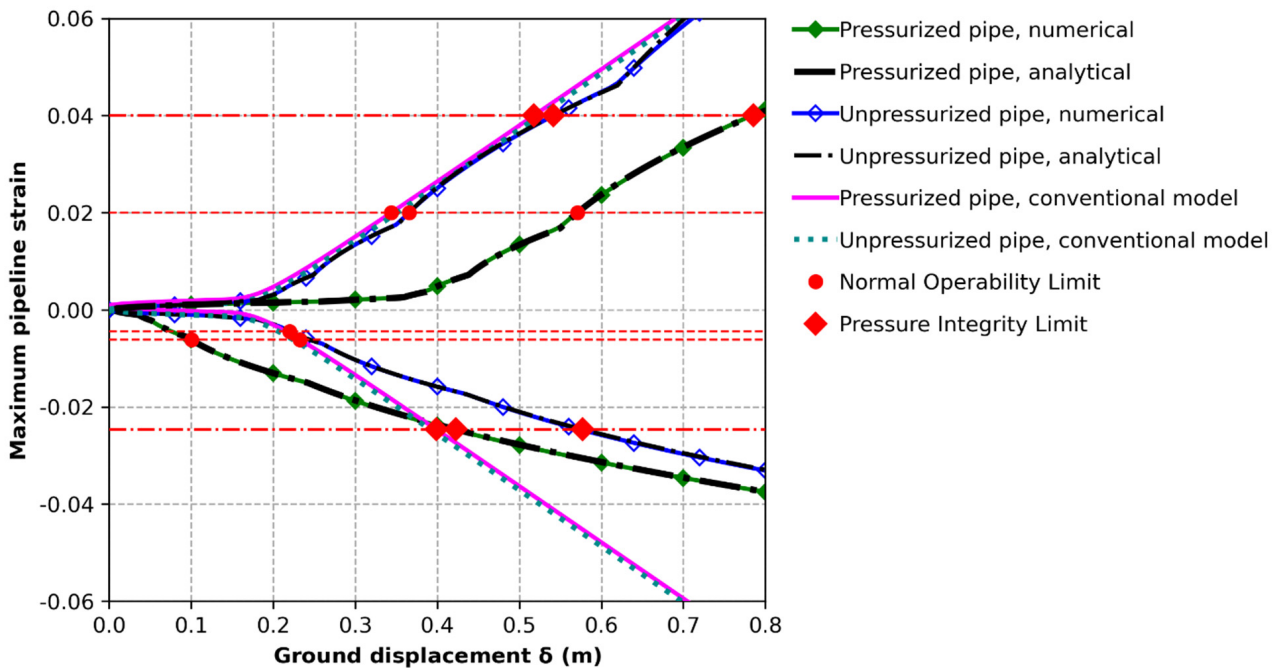


Figure 5. The comparison between the numerical, the conventional [8,11,13], and the proposed analytical models, evaluating the pipeline performance under longitudinal PGD ($L_b = 300$ m) in terms of maximum tensile and compressive pipe strain as a function of the ground displacement δ .

Table 4. The critical ground displacement $\delta_{cr,i}$ corresponding to the achievement of the normal operability (NOL) and pressure integrity (PI) limit states, for tension and compression, according to the numerical and analytical methods.

	Analysis Method	Normal Operability Limit		Pressure Integrity Limit	
		Tension δ_{t1} (m)	Compression δ_{c1} (m)	Tension δ_{t2} (m)	Compression δ_{c2} (m)
Pressurized pipeline	numerical	0.5706	0.0996	0.7835	0.4192
	analytical	0.5710	0.1001	0.7854	0.4226
	% difference	0.06%	0.51%	0.24%	0.81%
	conventional	0.3440	0.2327	0.5179	0.3988
	% difference	65.90%	−57.18%	51.30%	5.09%
Unpressurized pipeline	numerical	0.3656	0.2200	0.5420	0.5738
	analytical	0.3655	0.2199	0.5415	0.5773
	% difference	−0.02%	−0.06%	−0.08%	0.61%
	conventional	0.3511	0.2069	0.5249	0.3917
	% difference	4.12%	6.35%	3.24%	46.48%

Finally, the proposed analytical model, evaluating the response of the buried operating pipeline subjected to longitudinal PGD, can be implemented in most programming languages (e.g., Python, Matlab) for further parametric analyses.

2.4. Critical Soil Displacement (δ_{cr}) and Length (L_{cr}) for the Performance Limit States of the Operating Pipeline

As the soil displacement δ increases (case II), the maximum magnitude of the pipeline axial force and associated strain at both margins of the PGD zone increase monotonically (Equation (1)), until the soil reaction mobilizes fully over the entire soil block length L_b (case I). Herein, the total soil load ($f_s L_b$) over the PGD zone is resisted by the developed pipe axial force that is at a maximum at the head ($F_{t,max}$) and toe ($F_{c,max}$) of the sliding soil block. Therefore, the critical soil length L_{cr} , associated with full mobilization of the soil reaction (case I) for a given value of soil displacement δ , is directly proportional to the overall pipe load at the edges of the PGD zone:

$$L_{cr} = [F_{t,max}(\delta/2) - F_{c,max}(\delta/2)]/f_s \quad (5)$$

Consequently, the pipeline deformation demand will reach a certain limit state only if the soil displacement δ and block length L_b are equal or greater than the critical soil displacement $\delta_{cr,i}$ and length $L_{cr,i}$ corresponding to that performance criterion, respectively.

Figure 6 shows the variation of the critical soil block length L_{cr} as a function of the ground displacement δ , indicating the critical values associated with the achievement of the performance limit states in the pressurized ($P_i/P_{max} = 0.75$, $\Delta T = 50$ °C) and unpressurized pipelines ($P_i/P_{max} = 0$, $\Delta T = 0$ °C). Furthermore, the distributions of the axial strain, stress, force, displacement, and soil friction reaction along the pressurized and unpressurized pipelines for increasing values of applied ground movement δ are presented in Appendix A, illustrating the different system responses for case I and case II.

Clearly, the pipeline response depends on the operating loads, with the performance limit states in compression being reached for lower levels of critical soil displacement and length in the pressurized pipeline, compared to the unpressurized one.

Interestingly, the pressurized and unpressurized pipelines satisfy all the performance criteria for soil block lengths L_b that are shorter than 145 m and 254 m, respectively, for any value of the applied ground displacement, δ . Conversely, the pipeline will fail to satisfy any limit state for values of the soil block length L_b and ground displacement δ exceeding 280 m and 0.79 m, respectively (Figure 6).

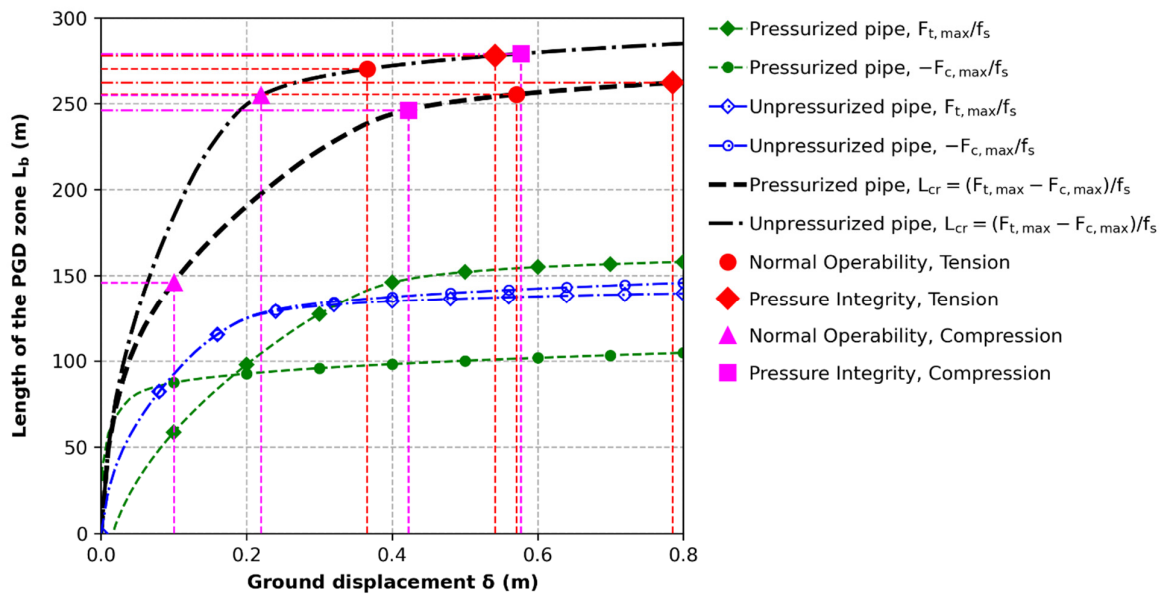


Figure 6. The variation of the critical soil block length, $L_{cr} = (F_{t,max} - F_{c,max})/f_s$, as a function of the ground displacement δ , with an indication of the critical values $(\delta_{cr,i}, L_{cr,i})$ associated with the achievement of the pipeline performance limit states.

Figures 7 and 8 show the maximum pipe strain magnitude as a function of the ground deformation demand (δ, L_b) , for the pressurized and unpressurized pipelines, respectively, highlighting the critical PGD values $(\delta_{cr,i}, L_{cr,i})$ corresponding to the achievement of the performance limit states.

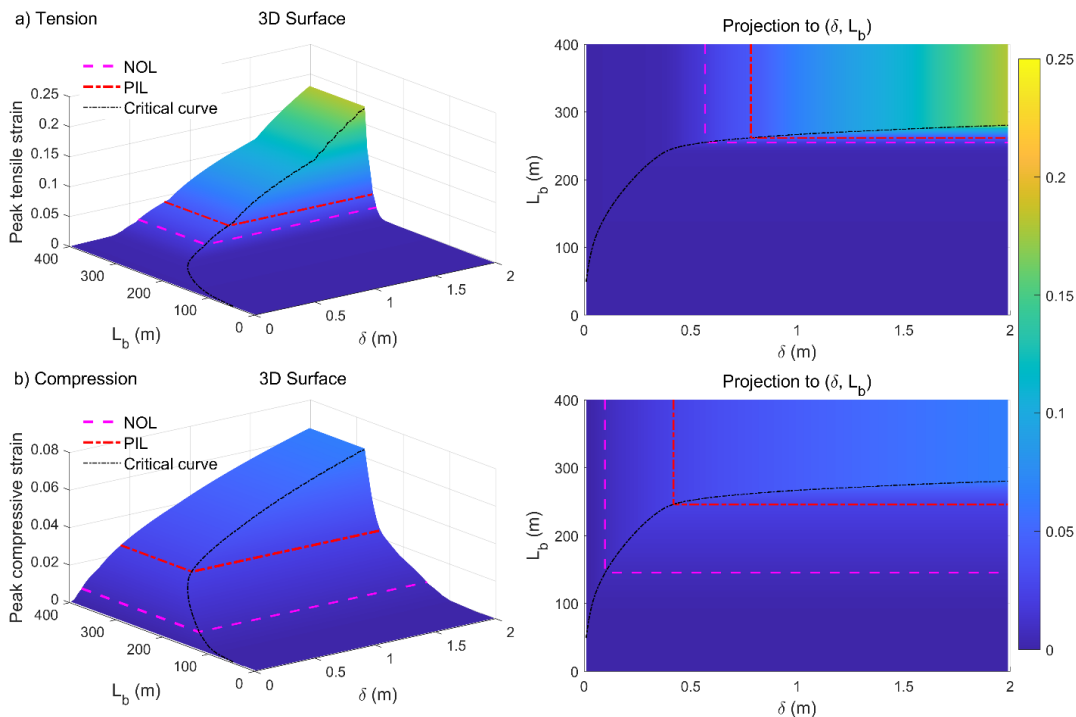


Figure 7. The peak axial strain magnitude in the pressurized pipeline ($P_i/P_{max} = 0.75, \Delta T = 50 \text{ }^\circ\text{C}$) as a function of the PGD length L_b and displacement δ for (a) tension and (b) compression. The dashed horizontal curves represent the strain isolines corresponding to the NOL and PIL performance limit states.

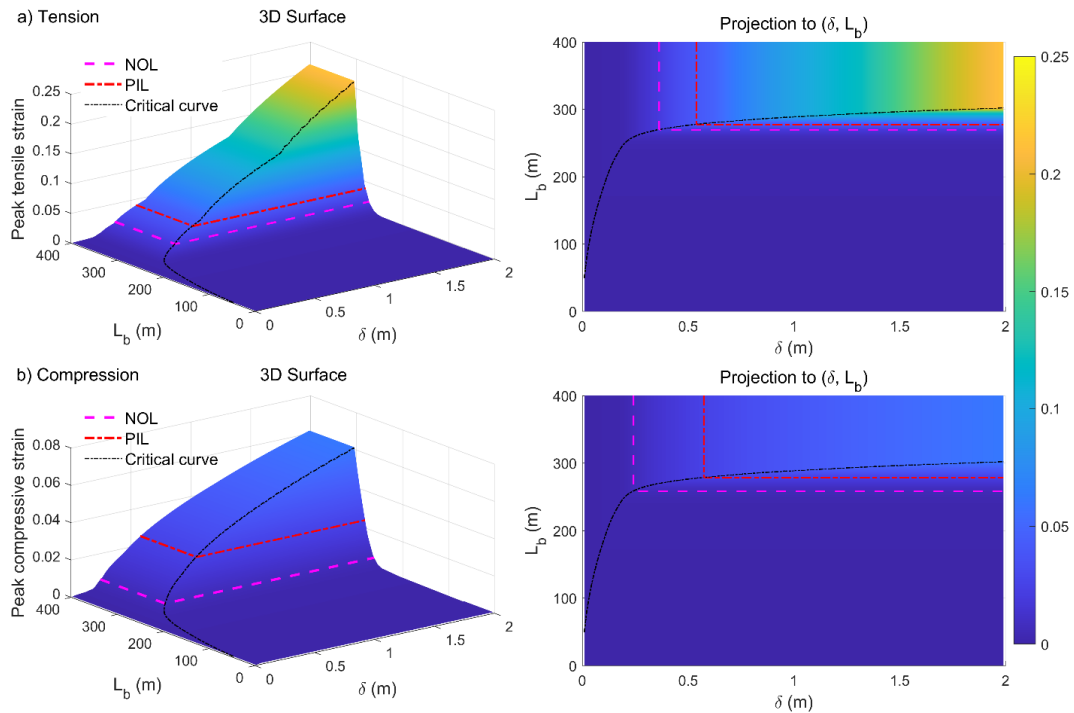


Figure 8. The peak axial strain magnitude in the unpressurized pipeline ($P_i/P_{max} = 0$, $\Delta T = 0$ °C) as a function of the PGD length L_b and displacement δ for (a) tension and (b) compression. The dashed horizontal curves represent the strain isolines corresponding to the NOL and PIL performance limit states.

Clearly, the curve of the critical soil block length L_{cr} as a function of the ground displacement δ (Figure 6) separates the PGD demand characterizing case I of short soil block ($\delta > \delta_{cr} \vee L_b < L_{cr}$) from that of case II of long soil block ($\delta < \delta_{cr} \vee L_b > L_{cr}$). Hence, the strain isolines are defined by two half-lines running parallel to the δ and L_b axis, intersecting on the critical curve, as shown in Figures 7 and 8.

2.5. Uncertainty Analysis

The deterministic analysis procedure adopted in the previous section assumes precise knowledge of the system parameters. However, all problem variables are characterized by a certain degree of uncertainty, including the material strength and the seismic loading. To quantify the effect of these uncertainties on the pipeline performance, this study develops a robust fragility analysis framework based on the Monte Carlo Simulation (MCS). The latter considers a large number of soil–pipeline system samples, generated by random sampling of the input system parameters, based on their probability distribution. The seismic demands are compared to the structural capacity values associated with each performance limit state, allowing us to estimate the associated probability of exceedance conditioned to the level of ground motion intensity measure, IM, represented by the vector (δ, L_b) .

Table 5 summarizes the input variables and their probability distribution. To investigate the effect of the soil cover depth H_c , three different values between 1.0 m and 2.0 m were considered, representative of typical onshore pipeline installations. The soil strength parameters, i.e., the longitudinal soil reaction per unit length of pipeline f_s , and relative soil–pipe displacement at friction sliding, u_0 are assumed to follow a normal distribution, with the mean values derived according to [31], and a coefficient of variation $COV = 30\%$ [26,35,36], as indicated in Table 5. The uncertainty of the X42 steel grade pipe material was modeled considering that the yield strength follows a normal distribution, with a mean value $\sigma_y = 290$ MPa and a small $COV = 3.5\%$ (Table 5), representing the low variability of the steel properties.

Table 5. Probabilistic characteristics of the input parameters.

	Parameter	Units	Distribution	Mean or Range	COV
Pipe	Internal pressure, P_i	KPa	Uniform	[0, 5846.4]	0.035
	Temperature variation, ΔT	°C	Uniform	[0, 50]	
	Yield strength, σ_y	MPa	Normal	290	
Soil	Cover depth, H_c	m	-	[1, 1.5, 2]	0.3
	Soil friction reaction per unit pipe length, f_s	KN/m	Normal	[19.2, 26.8, 34.4]	
	Relative soil–pipe displacement at friction sliding, u_0	mm	Normal	3	

The limit state functions for normal operability (NOL) and pressure integrity (PIL) for tension and compression are expressed in terms of the system demand (δ , L_b) and capacity ($\delta_{cr,i}$, $L_{cr,i}$) corresponding to each performance criteria:

$$g_{t1} = \max(\delta_{t1} - \delta, L_{b,t1} - L_b) \tag{6}$$

$$g_{c1} = \max(\delta_{c1} - \delta, L_{b,c1} - L_b) \tag{7}$$

$$g_{t2} = \max(\delta_{t2} - \delta, L_{b,t2} - L_b) \tag{8}$$

$$g_{c2} = \max(\delta_{c2} - \delta, L_{b,c2} - L_b) \tag{9}$$

The probability of exceeding the normal operability (NOL) and the pressure integrity limit (PIL) state, conditioned to the PGD intensity measure level (δ , L_b), is given by the joint union of the associated damage states for tension and compression:

$$P[\text{NOL} | (\delta, L_b)] = P[\max(g_{t1}, g_{c1}) \leq 0 | (\delta, L_b)] \tag{10}$$

$$P[\text{PIL} | (\delta, L_b)] = P[\max(g_{t2}, g_{c2}) \leq 0 | (\delta, L_b)] \tag{11}$$

These probabilities can be effectively calculated using the Monte Carlo Simulation (MCS) method, as summarized in Table 6.

Table 6. Summary of fragility function calculation framework, based on MCS.

1. Definition of the uncertain input parameters and their probability distributions.
2. Generation of a sample set of the random variables in the system, considering their probability distributions.
3. Evaluation of the pipeline displacement capacities for each strain limit corresponding to each performance criterion $\delta_{cr,i}$, using Equation (1) and the functional relationships in Table 2: $\delta_{cr,i} = 2\Delta L(\epsilon_{cr,i})$.
4. Evaluation of the critical soil lengths $L_{cr,i}$, using Equation (5) and the analytical formulation in Table 2 for calculating the pipeline force at the head ($F_{t,max}$) and toe ($F_{c,max}$) of the soil block: $L_{cr,i} = [F_{t,max}(\delta_{cr,i}/2) - F_{c,max}(\delta_{cr,i}/2)]/f_s$
5. Evaluation of the limit state functions, as the difference between the calculated system capacity ($\delta_{cr,i}$, $L_{cr,i}$) and demand (δ , L_b), using Equations (6)–(9).
6. Evaluation of the indicator functions, $I_{1i}(\delta, L_b) = \max(g_{t1}, g_{c1}) \leq 0$, and $I_{2i}(\delta, L_b) = \max(g_{t2}, g_{c2}) \leq 0$, which are equal to the unity under unsatisfactory performance for the normal operability and pressure integrity limit state, respectively, and are zero otherwise.
7. Repetition of steps (1) to (6) N times, to obtain N sample values of $I_{1i}(\delta, L_b)$, $I_{2i}(\delta, L_b)$, counting the unsatisfactory performance for the normal operability (NOL) and the pressure integrity limit (PIL) state, respectively.
8. Evaluation of the probability of exceedance of the normal operability (NOL) and the pressure integrity limit (PIL) state, for a given PGD demand (δ , L_b), as the ratio between the total sum of $I_{1i}(\delta, L_b)$ and $I_{2i}(\delta, L_b)$ to the sample size N :

$$P[\text{NOL} | (\delta, L_b)] = \frac{1}{N} \sum_{i=1}^N I_{1i}(\delta, L_b) \tag{12}$$

$$P[\text{PIL} | (\delta, L_b)] = \frac{1}{N} \sum_{i=1}^N I_{2i}(\delta, L_b) \tag{13}$$

The described algorithm can be easily implemented within most programming languages, like Python [37], to evaluate the fragility surfaces representing the conditional probability of the system reaching a performance limit state, as a function of the seismic demand.

3. Fragility Surfaces

This section presents the fragility analysis results of the buried operating steel pipelines subjected to longitudinal PGD, obtained using the methodology described in Section 2.5.

The evaluated fragility surfaces for the buried pipeline at a cover depth $H_c = 1.5$ m are shown in Figures 9a and 9b for the NOL and the PIL performance limit states, respectively.

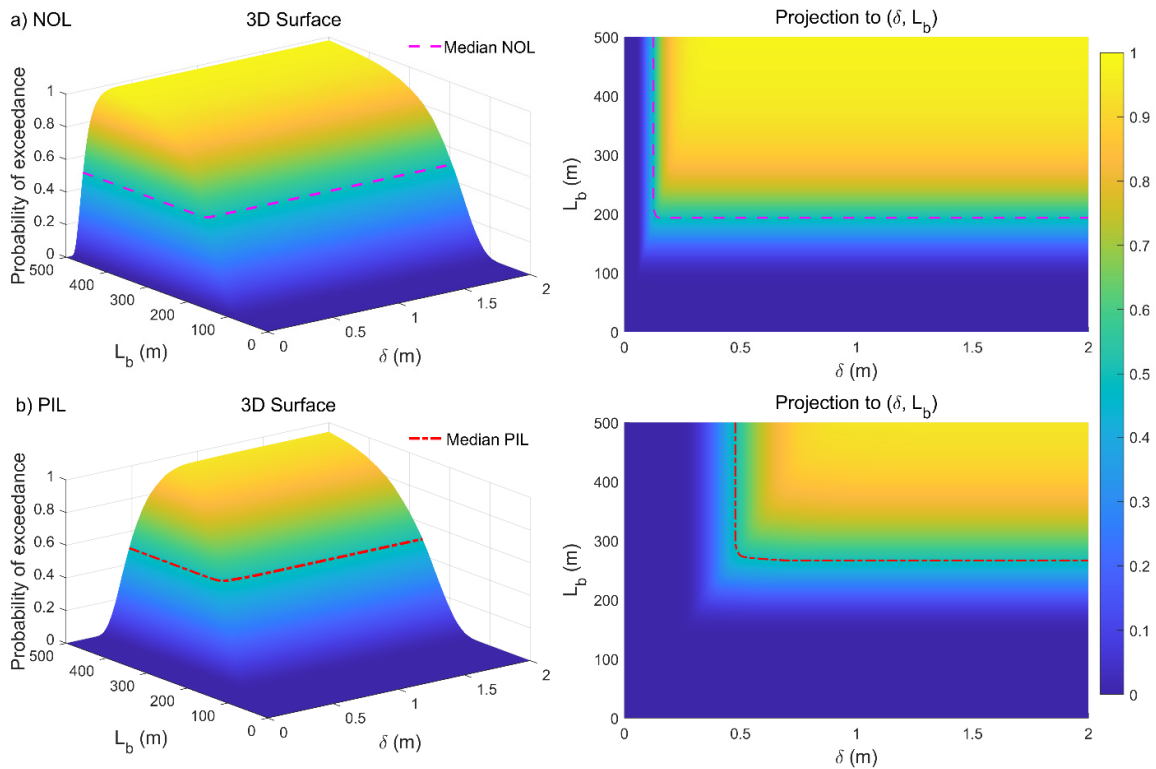


Figure 9. Fragility surface of buried pipeline ($H_c = 1.5$ m) for (a) Normal Operability Limit (NOL) and (b) Pressure Integrity Limit (PIL).

Clearly, the probability of the pipeline exceeding the performance criteria increases for larger soil displacements δ and lengths L_b , being greater for the NOL, compared to the PIL limit state. The iso-probability lines are defined by two half-lines parallel to the δ and L_b axis (Figure 9). This is consistent with the pipeline deformation response observed for the deterministic analysis (Figures 7 and 8), as schematically illustrated in Figure 10. Specifically, the median values of soil displacement (δ, L_b), corresponding to a 50% probability of reaching the NOL and PIL criteria are (0.13 m, 193.4 m) and (0.48 m, 267.4 m), respectively, as indicated in Table 7. These critical values are less than the ones evaluated deterministically for the unpressurized pipeline (Figure 6), particularly for the NOL performance limit state (Table 7). This may result in under-designed pipeline systems when using the deterministic approach, highlighting the importance of accurate uncertainty analysis for a reliable infrastructure design.

Table 7. Comparison of pipeline performance based on deterministic and fragility analysis results.

	H_c (m)	Deterministic Analysis			Fragility Analysis (Median Value)		
		1	1.5	2	1	1.5	2
NOL	$\delta_{cr,1}$ (m)	0.31	0.22	0.17	0.18	0.13	0.10
	$L_{cr,1}$ (m)	356.5	254.9	198.3	270.2	193.4	151.7
PIL	$\delta_{cr,2}$ (m)	0.76	0.54	0.42	0.67	0.48	0.38
	$L_{cr,2}$ (m)	388.9	278.0	216.3	372.5	267.4	208.4

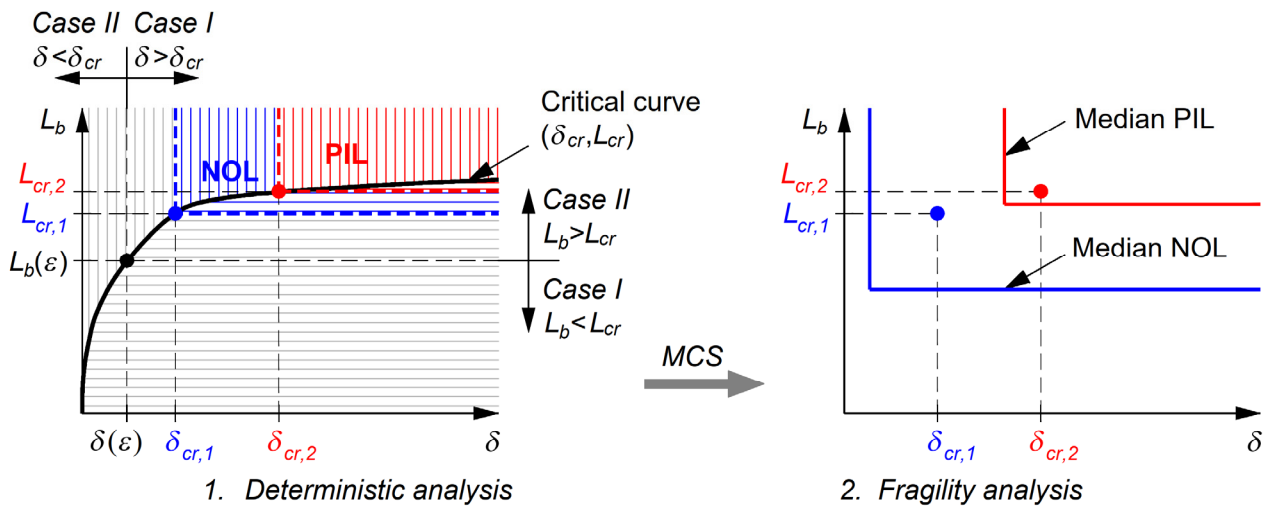


Figure 10. Schematic representation of the performance assessment of the buried pipeline subjected to the PGD demand (δ, L_b), using the deterministic and fragility analysis framework.

To investigate the effect of the cover depth H_c on pipeline performance, the fragility functions were evaluated considering a minimum cover depth value of $H_c = 1$ m and a maximum of $H_c = 2$ m (Figure 11). This results in a proportional variation in the soil friction reaction per unit pipe length f_s [31] that directly controls the pipeline deformation demand (Table 2).

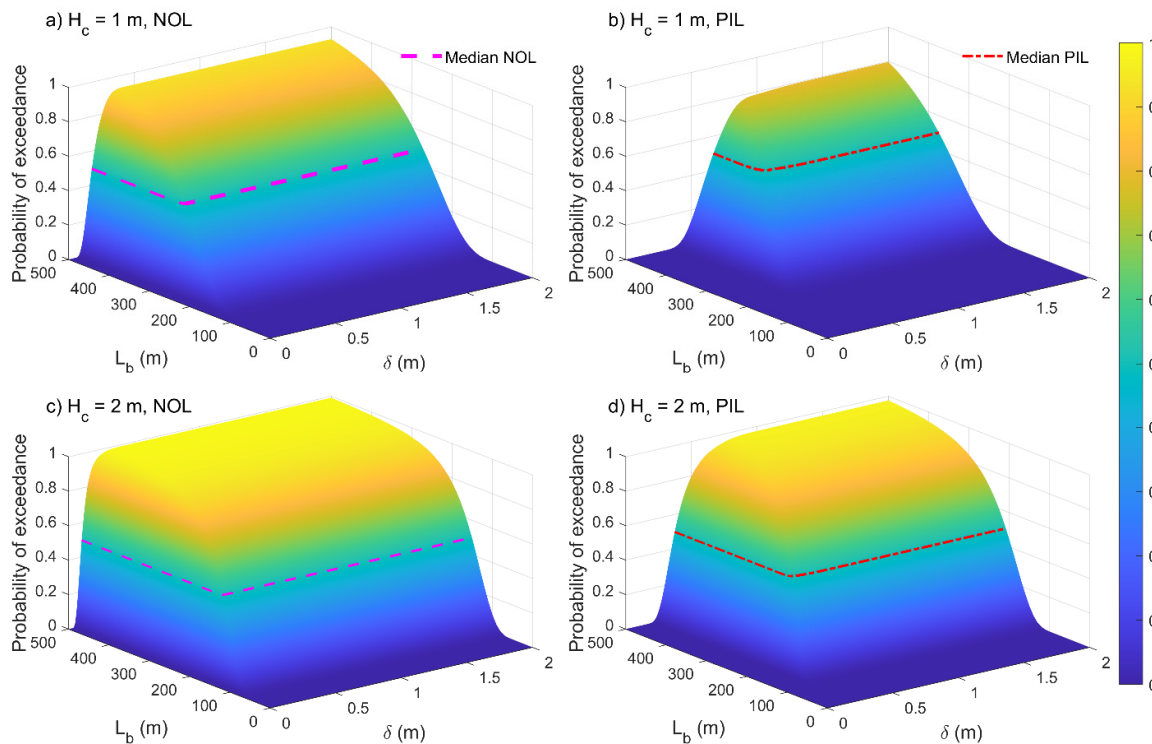


Figure 11. Fragility surface of buried pipeline for different cover depths and performance limit states: (a) $H_c = 1.0$ m, NOL; (b) $H_c = 1.0$ m, PIL and (c) $H_c = 2.0$ m, NOL; and (d) $H_c = 2.0$ m, PIL.

Clearly, the probability of the pipeline exceeding the performance limit states for a given amount of PGD (δ, L_b) increases with greater burial depths and associated soil friction reaction. Specifically, the median values of ground displacement intensity (δ, L_b), corresponding to a 50% probability of reaching the NOL criteria are (0.18 m, 270.2 m) and (0.10 m, 151.7 m) for the shallower ($H_c = 1$ m) and deeper ($H_c = 2$ m) soil cover depths,

respectively (Table 7). Likewise, a critical PGD demand (δ, L_b) of (0.67 m, 372.5 m) and (0.38 m, 208.4 m) is needed to achieve a 50% probability of reaching the PIL criteria for the former ($H_c = 1$ m) and latter ($H_c = 2$ m) pipe burial condition, respectively.

This is consistent with current pipeline design guidelines prescriptions, recommending the use of shallow burial depths, light-weight backfill, and pipe coating with a low friction coefficient to minimize the intensity of soil–pipeline interaction, optimizing the system performance [14,32].

The obtained fragility surfaces permit us to assess the probability of the pipeline exceeding the performance criteria, conditioned to the PGD demand (d, L_b), considering the effect of system uncertainties, including the varying operational loads.

4. Global Sensitivity Analysis

This section presents the results of the global sensitivity analysis (GSA) conducted to quantify the uncertainty (variance) of the model prediction $y = g(x_1, x_2, \dots, x_m)$, attributed to each input random variable x_i . This method has the advantage of considering the sensitivity over the entire input space, including the nonlinear interaction effects between the system variables, allowing us to identify those parameters that have the greatest influence on the model output.

The adopted GSA procedure is based on the Sobol’s variance decomposition method, in which the total variance of model output $V = Var(y)$ is decomposed into component variances resulting from individual parameters V_i and their interactions V_{ijk} [38].

Specifically, the first-order Sobol index S_i of an input variable x_i represents the fraction of the output variance attributed to x_i ($S_i = V_i/V$), while the higher order Sobol indices S_{ijk} indicate the impact of input parameter interactions on the output results ($S_{ijk} = V_{ijk}/V$). Finally, the total-order index S_{Ti} quantifies the overall effects of one input parameter x_i including its interactions with all other variables on the model output, and is defined as the sum of all sensitivity indices involving x_i ($S_{Ti} = S_i + \sum_{i \neq j} S_{ij} + \sum_{i \neq j \neq k} S_{ijk} + \dots$).

To accurately estimate the first-order and total Sobol indices this study performs a double-loop Monte Carlo integration procedure [39].

The estimated influence of the input random variables on the achievement of the pipeline performance limit states, based on Sobol’s sensitivity indexes, is shown in Figure 12.

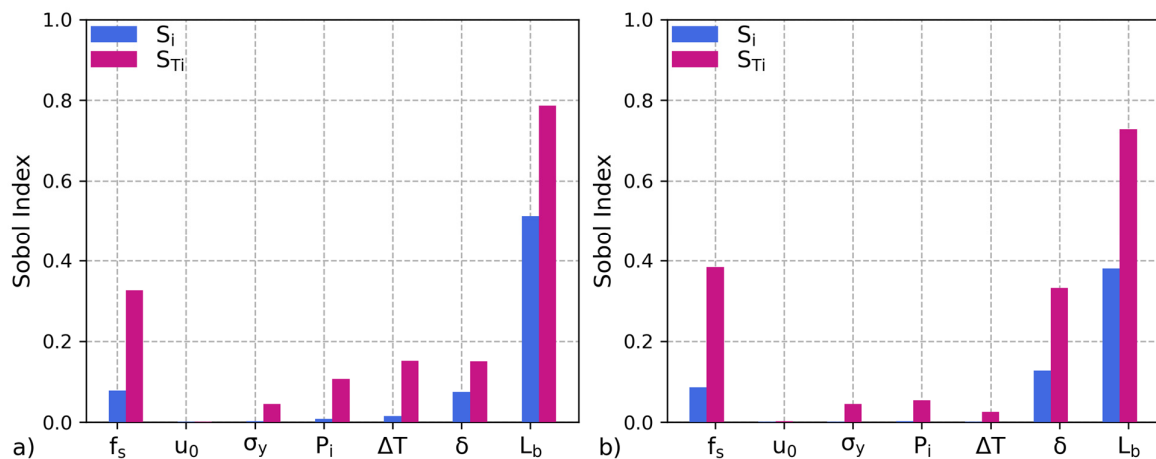


Figure 12. The comparison of the first-order and total-order sensitivity indices of the system input parameters for the (a) NOL and (b) PIL performance limit states.

The soil block length L_b is the most influential parameter, with a first-order sensitivity index S_i of 51.2% and 38.1% for the NOL and PIL limit states, respectively, and a total sensitivity index S_{Ti} greater than 72% for both performance limit states. This is evident, since the length of the PGD zone L_b controls the pipeline deformation demand, where each limit state is achieved provided that the soil block length value exceeds the corresponding critical threshold ($L_b \geq L_{cr,i}$).

The second most significant variable is the soil friction reaction per unit pipe length f_s , with a first-order sensitivity index S_i of 7.8% and 8.7% for the NOL and PIL limit states, respectively, and a total sensitivity index S_{Ti} greater than 32% for both damage levels. The third most influential parameter for the PIL limit state is the soil displacement δ , with an associated first-order sensitivity index S_i of 12.8% and a total sensitivity index S_{Ti} of 33.2%.

Interestingly, the pipeline operating temperature is the third most influential parameter for the NOL limit state, with a first-order sensitivity index S_i and a total sensitivity index S_{Ti} of 1.6% and 15.2%, respectively. This is consistent with the sensitivity analysis results reported in [25], quantifying the effect of uncertainties of the pipeline system subjected to longitudinal PGD, including the significant impact of operational loads.

While the first-order sensitivity indices for the internal pressure P_i , are negligible ($S_i < 1\%$), the total sensitivity index S_{Ti} reaches 10.7% and 5.5% for the NOL and PIL limit states, respectively, highlighting the considerable interaction effects of P_i with the other input variables.

The least influential input random variables are the pipe yield strength σ_y and relative soil–pipe displacement at friction sliding u_0 , with an associated total sensitivity index S_{Ti} less than 4.5% and 0.3%, respectively. This can be attributed to the low variability assumed for the steel yield strength, and the negligible effect of the elastic stiffness in the soil–pipeline interaction for a large PGD, respectively. This is consistent with the sensitivity analysis results reported in [25] and the simplified assumptions adopted in existing analytical models of buried pipelines under longitudinal PGD, which conservatively neglect the relative soil–pipeline displacement at friction sliding u_0 [11].

The use of both sensitivity indices allows a comprehensive understanding of the influence of the input variables on the performance limit state function, highlighting the importance of interaction effects between the soil–pipeline system parameters.

5. Conclusions

This study develops a new analytical model that accurately and efficiently evaluates the performance of buried operating pipelines under longitudinal PGD, considering the asymmetric pipeline response- to tension and compression under varying operational loads.

A further comparison of the proposed analytical model to the detailed finite element analysis results showed excellent agreement, demonstrating its capacity to accurately assess the pipeline response as a function of the system parameters, including the operational pressure and temperature variations. The analytical model was efficiently implemented within a robust fragility function calculation framework based on MCS, allowing us to assess the probability of exceedance of the pipeline performance limit states conditioned to the PGD demand (δ, L_b), considering the system uncertainties.

The evaluated fragility surfaces showed that the probability of the pipeline reaching the performance criteria increases for larger soil displacement δ and lengths L_b , as well as cover depths H_c , because of the greater mobilized soil reaction counteracting pipeline deformation. This requires implementation of proper engineering design solutions that minimize the risk of pipeline damage, for example, by adopting shallow soil cover depths, light weight backfill, and low-friction pipe coating.

The performed GSA allowed us to quantify the uncertainty of the pipeline performance assessment attributed to each random system parameter, considering the sensitivity over the entire input space, including the nonlinear interaction effects between variables. The PGD length (L_b) was the most influential parameter with respect to the exceedance of the NOL and PIL performance limit states, followed by the soil friction per unit pipe length (f_s) and ground displacement (δ), based on the first-order and total-order Sobol indices. This is consistent with the expected system performance, since the intensity of the PGD and soil–pipeline interaction directly control the pipeline deformation demand.

The significant total sensitivity indices of the temperature variation (ΔT) and internal pressure (P_i) for the NOL limit state demonstrated the importance of the effects of their interaction with the other input variables. Both the deterministic and uncertainty analysis

results highlighted the impact of operational loads on pipeline performance, which need to be accurately considered in pipeline system modeling and design. The comparison between the deterministic and fragility analysis results showed that neglecting the variability of the system parameters, including operational loads, may result in under-designed pipelines, highlighting the importance of uncertainty analysis for a reliable infrastructure design.

Overall, the proposed analytical fragility function calculation framework provides a useful methodology for effectively assessing the performance of operating pipelines under longitudinal PGD, quantifying the effects of the critical parameters impacting system response.

Funding: This research received no external funding.

Data Availability Statement: The original contributions presented in the study are included in the article, further inquiries can be directed to the corresponding author.

Acknowledgments: This publication is made possible in part by support from the Berkeley Research Impact Initiative (BRII) sponsored by the UC Berkeley Library, that is greatly acknowledged. The author would like to thank Kenichi Soga, Thomas D. O'Rourke, Ziqi Wang and Sang-ri Yi at the Department of Civil and Environmental Engineering of UC Berkeley for valuable discussions.

Conflicts of Interest: The authors declare no conflict of interest.

Appendix A

This appendix presents the seismic performance of the pressurized and unpressurized pipelines analyzed in Section 2.3 in terms of axial strain, stress, force, displacement, and soil friction reaction along their axes for increasing values of ground movement δ , for case I and case II.

The moving soil block induces localized relative soil–pipeline displacement at the margins of the PGD zone and associated resistance forces. This results in a maximum pipeline axial force at the sliding block head and maximum axial compression force at the toe, decreasing linearly thereupon due to the sliding soil friction (f_s). Beyond this zone, the relative soil–pipeline displacement is negligible, and the pipeline displacement matches that of the ground until the soil reaction mobilizes fully along the entire soil block length L_b (case I), remaining constant thereafter.

The length of the PGD L_b is a critical geotechnical parameter, determining whether the pipeline performance criteria are exceeded for increasing ground displacements δ , as shown in Figures A1 and A2, indicating the pressurized and unpressurized pipe response, respectively, for $L_b = 200$ m (case I). Conversely, the responses of the pressurized and unpressurized pipelines subjected to long soil block movement ($L_b = 300$ m) are shown in Figures A3 and A4, respectively.

The operating pipeline exhibits an asymmetric response along its axis in tension and compression, compared to the non-operating pipeline, as evident from the resulting axial force, stress, strain, displacement, and soil friction reaction indicated in Figures A1–A4.

The maximum pipeline displacement corresponding to full mobilization of the soil reaction for the pressurized and unpressurized pipelines under short soil block ($L_b = 200$ m) movement is equal to 0.12 m (Figure A1) and 0.23 m (Figure A2), respectively. This is consistent with the critical ground displacement and associated soil block length values (δ, L_b) shown in Figure 6. The pressurized pipeline reaches the compressive strain limit for the NOL criteria (0.62%) for a soil displacement of 0.1 m (Figure A1d), whereas the unpressurized pipeline remains elastic, with a maximum axial strain of 0.11% (Figure A2d). This further highlights the influence of the operating loads on pipeline performance, as discussed throughout the paper.

For case II ($L_b = 300$ m), the pressurized and unpressurized pipelines exceed the PIL limit state for a ground displacement δ of 0.42 m (Figure A3) and 0.57 m (Figure A4), respectively, confirming the detrimental effect of these operating loads on pipeline performance, as observed in Section 2.4.

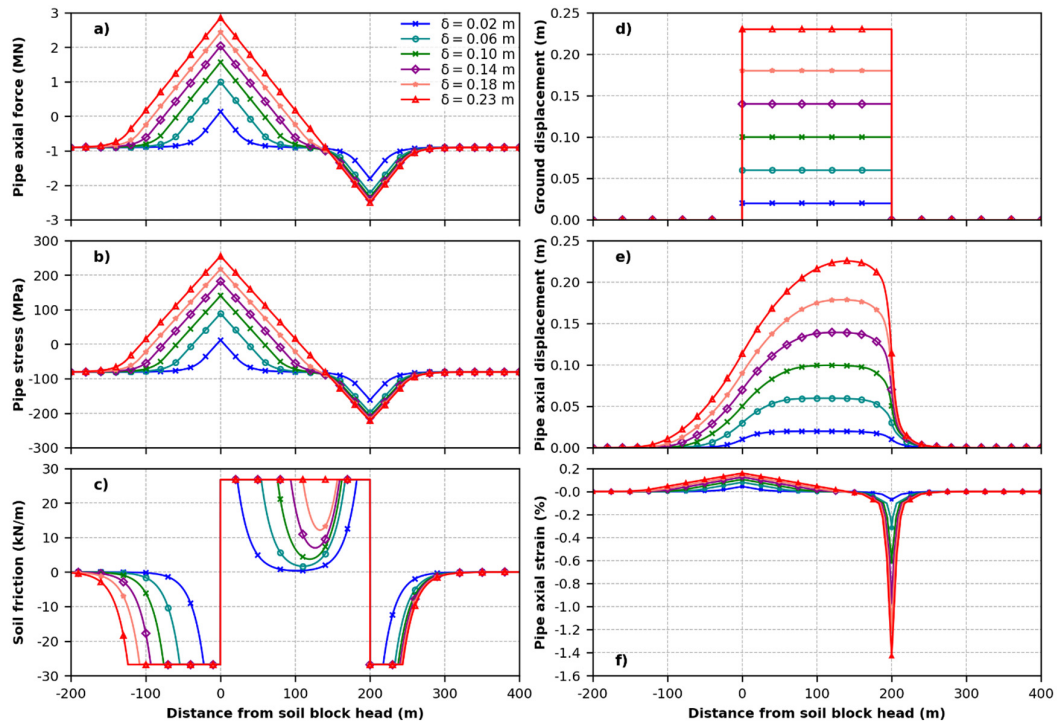


Figure A1. Response of the pressurized pipeline ($P_i/P_{max} = 0.75$, $\Delta T = 50\text{ }^\circ\text{C}$) to longitudinal PGD with block length $L_b = 200\text{ m}$ (case I): (a) pipe axial force; (b) pipe axial stress; (c) soil friction; (d) ground displacement; (e) pipe axial displacement; (f) pipe axial strain vs. distance from tension crack.

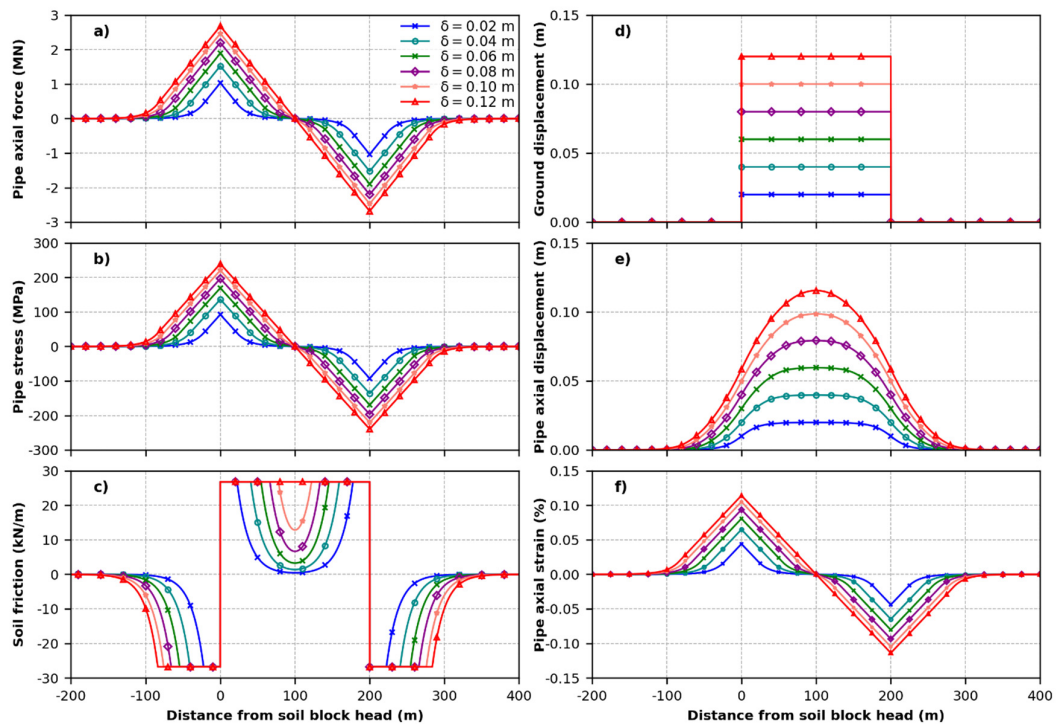


Figure A2. Response of the unpressurized pipeline ($P_i/P_{max} = 0$, $\Delta T = 0\text{ }^\circ\text{C}$) to longitudinal PGD with block length $L_b = 200\text{ m}$ (case I): (a) pipe axial force; (b) pipe axial stress; (c) soil friction; (d) ground displacement; (e) pipe axial displacement; (f) pipe axial strain vs. distance from tension crack.

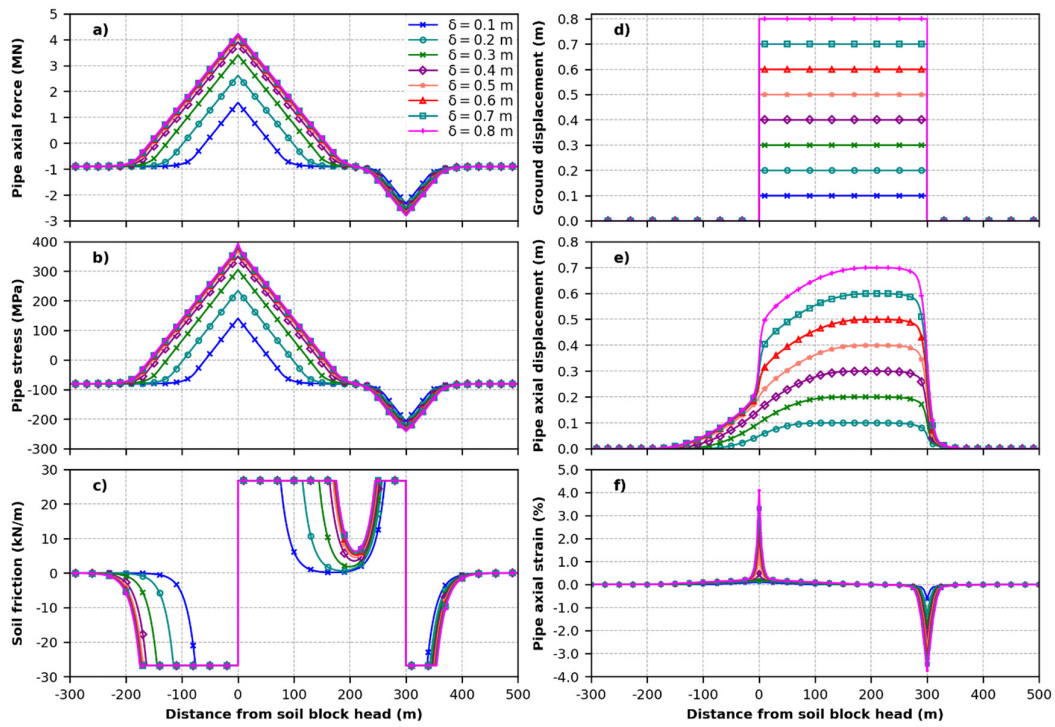


Figure A3. Response of the pressurized pipeline ($P_i/P_{max} = 0.75$, $\Delta T = 50$ °C) to longitudinal PGD with block length $L_b = 300$ m (case II): (a) pipe axial force; (b) pipe axial stress; (c) soil friction; (d) ground displacement; (e) pipe axial displacement; (f) pipe axial strain vs. distance from tension crack.

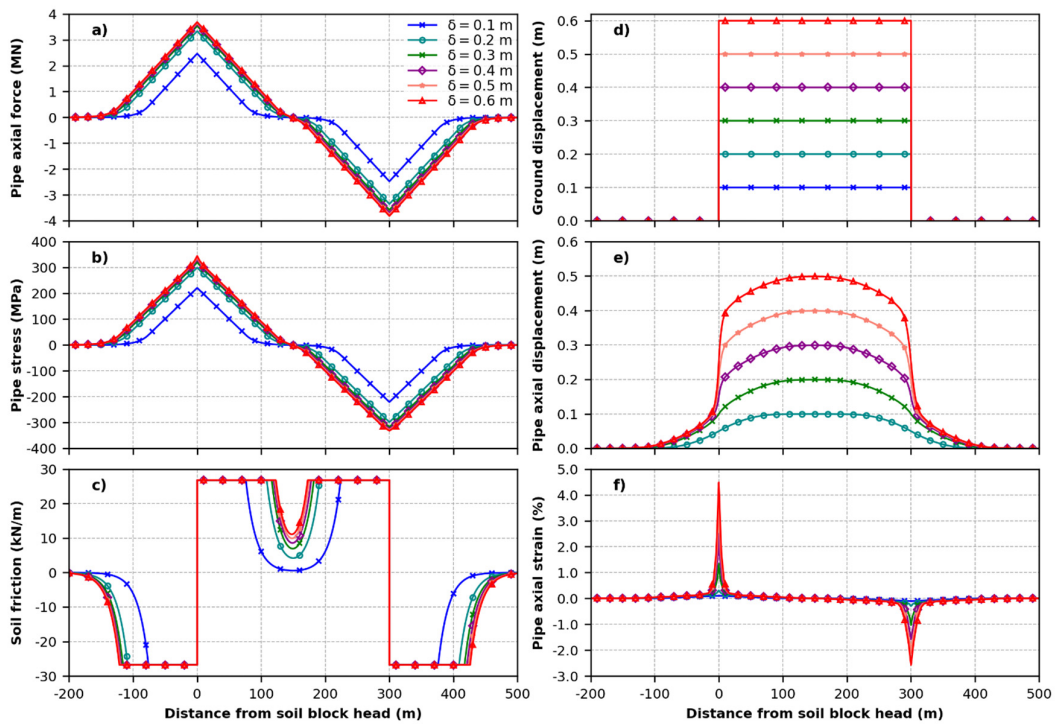


Figure A4. Response of the pressurized pipeline ($P_i/P_{max} = 0$, $\Delta T = 0$ °C) to longitudinal PGD with block length $L_b = 300$ m (case II): (a) pipe axial force; (b) pipe axial stress; (c) soil friction; (d) ground displacement; (e) pipe axial displacement; (f) pipe axial strain vs. distance from tension crack.

References

1. Kennedy, R.P.; Williamson, R.A.; Chow, A.M. Fault movement effects on buried oil pipeline. *Transp. Eng. J. ASCE* **1977**, *103*, 617–633. [[CrossRef](#)]
2. Karamitros, D.K.; Bouckovalas, G.D.; Kouretzis, G.P.; Gkesouli, V. An analytical method for strength verification of buried steel pipelines at normal fault crossings. *Soil Dyn. Earthq. Eng.* **2011**, *31*, 1452–1464. [[CrossRef](#)]
3. Trifonov, O.V.; Cherniy, V.P. Elastoplastic stress–strain analysis of buried steel pipelines subjected to fault displacements with account for service loads. *Soil Dyn. Earthq. Eng.* **2012**, *33*, 54–62. [[CrossRef](#)]
4. Sarvanis, G.C.; Karamanos, S.A. Analytical model for the strain analysis of continuous buried pipelines in geohazard areas. *Eng. Struct.* **2017**, *152*, 57–69. [[CrossRef](#)]
5. Banushi, G.; Squeglia, N. Seismic analysis of a buried operating steel pipeline with emphasis on the equivalent-boundary conditions. *J. Pipeline Syst. Eng. Pract.* **2018**, *9*, 04018005. [[CrossRef](#)]
6. O'Rourke, M.; Nordberg, G. Analysis procedures for buried pipelines subject to longitudinal and transverse permanent ground deformation. In Proceedings of the 3rd Japan–US Workshop on Earthquake Resistant Design of Lifeline Facilities and Countermeasures for Soil Liquefaction, San Francisco, CA, USA, 1 February 1991; Technical Report NCEER-91-0001. Multidisciplinary Center for Earthquake Engineering Research: Buffalo, NY, USA, 1991; pp. 439–453.
7. O'Rourke, M.J.; Nordberg, C. Behavior of buried pipelines subject to permanent ground deformation. In Proceedings of the 10th World Conference on Earthquake Engineering, Madrid, Spain, 19–24 July 1992; International Association for Earthquake Engineering: Dallas, TX, USA, 1992; pp. 5411–5416.
8. O'Rourke, M.J.; Liu, X. *Seismic Design of Buried and Offshore Pipelines*; Technical Report MCEER-12-MN04; Multidisciplinary Center for Earthquake Engineering: Buffalo, NY, USA, 2012; p. 380.
9. Suzuki, N.; Hagio, A. Safety assessment of welded pipelines undergoing large ground deformation. In Proceedings of the International Conference on Pipeline Design and Installation, Las Vegas, NV, USA, 25–27 March 1990; pp. 108–119.
10. O'Rourke, M.J.; Nordberg, C. *Longitudinal Permanent Ground Deformation Effects on Buried Continuous Pipelines*; Technical Report NCEER-92-0014; National Center for Earthquake Engineering Research: Buffalo, NY, USA, 1992; p. 120.
11. O'Rourke, M.J.; Liu, X.J.; Flores-Berrones, R. Steel pipe wrinkling due to longitudinal permanent ground deformation. *J. Transp. Eng.* **1995**, *121*, 443–451. [[CrossRef](#)]
12. American Lifelines Alliance. *Seismic Guidelines for Water Pipelines*; American Lifelines Alliance: Washington, DC, USA, 2005.
13. National Information Center of Earthquake Engineering. *IITK-GSDMA Guidelines for Seismic Design of Buried Pipelines; Provisions with Commentary and Explanatory Examples*; NICEE Publications: Kanpur, India, 2007.
14. 23/30479680 DC: BS EN 1998-4 Eurocode 8; Design of Structures for Earthquake Resistance: Part 4. Silos, Tanks and Pipelines, Towers, Masts and Chimneys. British Standards Institute: London, UK, 2023.
15. Toprak, S.; Cetin, O.A.; Nacaroglu, E.; Koc, A.C. Pipeline performance under longitudinal permanent ground deformation. In Proceedings of the 14th European Conference on Earthquake Engineering, Ohrid, North Macedonia, 30 August–3 September 2010.
16. Wijewickreme, D.; Honegger, D.; Mitchell, A.; Fitzell, T. Seismic vulnerability assessment and retrofit of a major natural gas pipeline system: A case history. *Earthq. Spectra* **2005**, *21*, 539–567. [[CrossRef](#)]
17. Wham, B.P.; Davis, C.A. Buried continuous and segmented pipelines subjected to longitudinal permanent ground deformation. *J. Pipeline Syst. Eng. Pract.* **2019**, *10*, 04019036. [[CrossRef](#)]
18. Banushi, G.; Wham, B.P. Deformation capacity of buried hybrid-segmented pipelines under longitudinal permanent ground deformation. *Can. Geotech. J.* **2021**, *58*, 1095–1117. [[CrossRef](#)]
19. Bain, C.A.; O'Rourke, T.D.; Bray, J.D. Pipeline Response to Seismic Displacement at Balboa Boulevard during the 1994 Northridge Earthquake. *J. Geotech. Geoenviron. Eng.* **2024**, *150*, 04023139. [[CrossRef](#)]
20. C-CORE; D.G. Honegger Consulting; SSD Inc. *Guidelines for Constructing Natural Gas and Liquid Hydrocarbon Pipelines Through Areas Prone to Landslide and Subsidence Hazards*; Design, Materials, and Construction Committee of Pipeline Research Council International, Inc.: Chantilly, VA, USA, 2009.
21. Schaumann, P.; Keindorf, C.; Brüggemann, H. Elasto-plastic bearing behavior of steel pipes exposed to internal pressure and bending. In Proceedings of the ISOPE International Ocean and Polar Engineering Conference, Seoul, Republic of Korea, 19 June 2005.
22. Honegger, D.G.; Wijewickreme, D.; Youd, T.L. Regional pipeline vulnerability assessment based upon probabilistic lateral spread hazard characterization. In Proceedings of the 10th National Conference on Earthquake Engineering, Anchorage, AK, USA, 21–25 July 2014; EERI: Oakland, CA, USA, 2014.
23. Banushi, G.; Squeglia, N.; Thiele, K.; Salvatore, W. Finite element analysis of operating buried pipelines subjected to strike-slip fault movement. In Proceedings of the 12th Pipeline Technology Conference, Berlin, Germany, 2–4 May 2017; EITEP Institute: Hannover, Germany, 2017.
24. Banushi, G.; Squeglia, N.; Thiele, K. Innovative analysis of a buried operating pipeline subjected to strike-slip fault movement. *Soil Dyn. Earthq. Eng.* **2018**, *107*, 234–249. [[CrossRef](#)]
25. Tsatsis, A.; Alvertos, A.; Gerolymos, N. Fragility analysis of a pipeline under slope failure-induced displacements occurring parallel to its axis. *Eng. Struct.* **2022**, *262*, 114331. [[CrossRef](#)]
26. Zhou, W. Reliability of pressurized pipelines subjected to longitudinal ground movement. *Struct. Infrastruct. Eng.* **2012**, *8*, 1123–1135.

27. Toprak, S.; Cirmiktili, O.Y. Reliability-Based Analyses and Design of Pipelines' Underground Movements during Earthquakes. In *Reliability-Based Analysis and Design of Structures and Infrastructure*; Farsangi, E.N., Noori, M., Gardoni, P., Takewaki, I., Varum, H., Bogdanovic, A., Eds.; CRC Press: Boca Raton, FL, USA, 2021; pp. 365–380.
28. Elnashai, A.S.; Di Sarno, L. *Fundamentals of Earthquake Engineering: From Source to Fragility*, 2nd ed.; Wiley and Sons: Chichester, UK, 2015; p. 496.
29. Di-Sarno, L.; Elnashai, A.S. Seismic Fragility Relationships for Structures. In *Advances in Assessment and Modeling of Earthquake Loss*; Akkar, S., Ilki, A., Goksu, C., Erdik, M., Eds.; Springer International Publishing: Cham, Switzerland, 2021; pp. 189–222.
30. Banushi, G. Seismic Design of Buried Steel Pipelines. Ph.D. Thesis, Technische Universität Braunschweig, Braunschweig, Germany, 2017. [[CrossRef](#)]
31. ALA (American Lifelines Alliance). *Guidelines for the Design of Buried Steel Pipe*; FEMA: Washington, DC, USA, 2001.
32. Honegger, D.G.; Nyman, D. *PRCI Guidelines for the Seismic Design and Assessment of Natural Gas and Liquid Hydrocarbon Pipelines*; Pipeline Research Council International, Technical Toolboxes: Houston, TX, USA, 2004.
33. ABAQUS. *User's Guide*; Simulia: Providence, RI, USA, 2022.
34. *ASME B31.4*; Pipeline Transportation Systems for Liquid Hydrocarbons and Other Liquids. ASME: New York, NY, USA, 2002.
35. Popescu, R.; Deodatis, G.; Nobahar, A. Effects of random heterogeneity of soil properties on bearing capacity. *Probabilistic Eng. Mech.* **2005**, *20*, 324–341. [[CrossRef](#)]
36. Ni, P.; Mangalathu, S.; Yi, Y. Fragility analysis of continuous pipelines subjected to transverse permanent ground deformation. *Soils Found.* **2018**, *58*, 1400–1413. [[CrossRef](#)]
37. Van Rossum, G. *Python 2.7.10 Language Reference*; Samurai Media Limited: London, UK, 2015.
38. Sobol', I.M. Sensitivity estimates for nonlinear mathematical models. *Math. Model.* **1990**, *2*, 112–118.
39. Saltelli, A. Making best use of model evaluations to compute sensitivity indices. *Comput. Phys. Commun.* **2002**, *145*, 280–297. [[CrossRef](#)]

Disclaimer/Publisher's Note: The statements, opinions and data contained in all publications are solely those of the individual author(s) and contributor(s) and not of MDPI and/or the editor(s). MDPI and/or the editor(s) disclaim responsibility for any injury to people or property resulting from any ideas, methods, instructions or products referred to in the content.